Nonlinear microstructured material to reduce noise and vibrations at low frequencies

Deborah Lavazec, Gwendal Cumunel, Denis Duhamel, Christian Soize, Anas Batou

Nonlinear Microstructured Material to Reduce Noise and Vibrations at Low Frequencies

Deborah Lavazec[1,2], Gwendal Cumunel[1], Denis Duhamel[1], Christian Soize[2] and Anas Batou[2]

1 Université Paris-Est, Laboratoire Navier, ENPC/IFSTTAR/CNRS, 6 et 8 Avenue Blaise Pascal, Cité Descartes, Champs-sur-Marne, 77455 Marne La Vallée Cedex 2, France
2 Université Paris-Est, Laboratoire Modélisation et Simulation Multi Echelle, MSME UMR 8208 CNRS, 5 bd Descartes, 77454 Marne-la-Vallée, France

E-mail: `deborah.lavazec@univ-paris-est.fr`

Abstract. At low frequencies, for which the wavelengths are wide, the acoustic waves and the mechanical vibrations cannot easily be reduced in the structures at macroscale by using dissipative materials, contrarily to the middle- and high-frequency ranges. The final objective of this work is to reduce the vibrations and the induced noise on a broad low-frequency band by using a microstructured material by inclusions that are randomly arranged in the material matrix. The dynamical regimes of the inclusions will be imposed in the nonlinear domain in order that the energy be effectively pumped over a broad frequency band around the resonance frequency, due to the nonlinearity. The first step of this work is to design and to analyze the efficiency of an inclusion, which is made up of a hollow frame including a point mass centered on a beam. This inclusion is designed in order to exhibit nonlinear geometric effects in the low-frequency band that is observed. For this first step, the objective is to develop the simplest mechanical model that has the capability to roughly predict the experimental results that are measured. The second step, which is not presented in the paper, will consist in developing a more sophisticated nonlinear dynamical model of the inclusion. In this paper, devoted to the first step, it is proved that the nonlinearity induces an attenuation on a broad frequency band around the resonance, contrarily to its linear behavior for which the attenuation is only active in a narrow frequency band around the resonance. We will present the design in terms of geometry, dimension and materials for the inclusion, the experimental manufacturing of this system realized with a 3D printing system, and the experimental measures that have been performed. We compare the prevision given by the stochastic computational model with the measurements. The results obtained exhibit the physical attenuation over a broad low-frequency band, which were expected.

1. Introduction

Among the first papers devoted to the energy pumping by simple oscillators, the works by Frahm [1] and by Roberson [2] can be cited. Since these pioneering works, the developments of metamaterials for absorbing vibrations and noise have recently received a great attention and numerous papers have been published, as for instance, [3, 4, 5, 6, 7, 8, 9, 10, 11, 12, 13, 14, 15, 16]. Concerning the energy pumping by linear or nonlinear mechanical oscillators in order to attenuate vibrations and noise for discrete or continuous systems at macro- or at micro-scales, many works have been published such as [17, 18, 19, 20, 21, 22, 23, 24, 25, 26, 27, 28].

This paper is devoted to the reduction of vibrations and induced noise in structures at macro-scale for the low-frequency band for which the first structural modes are excited. It is well known that the dissipative passive materials are not really efficient for this case contrarily to their efficiency in the middle and high frequencies. The final objective of this work is to reduce vibrations and induced noise on a broad low-frequency band by using a microstructured material by inclusions that are randomly arranged in the material matrix. The first step of this work is to design and to analyze the efficiency of an inclusion, which is made up of a hollow frame including a point mass centered on a beam. This inclusion behaves as a nonlinear oscillator that is designed in order that the energy pumping be efficient on a broad frequency band around its resonance instead of a narrow frequency band as for a linear oscillator. For this first step, the objective is to develop the simplest mechanical model that has the capability to roughly predict the experimental results that are measured. The second step will consist in developing a more sophisticated nonlinear dynamical system. In this paper, devoted to the first step, it is proved that the nonlinearity induced an attenuation on a broad frequency band around its resonance, whereas the associated linear system yields a reduction only on a narrow frequency band. We will present the design in terms of geometry, dimension and materials for the inclusion, the experimental manufacturing of this system realized with a 3D printed system, and the experimental measures that have been performed. We compare the prevision given by the stochastic computational model with the measurements. The results obtained exhibit the physical attenuation over a broad low-frequency band, which were expected.

2. Design of the inclusion, experimental manufacturing, and material identification
An inclusion has been designed at a macro-scale. It is made up of a point mass constituted of a cube with a hole, centered on a beam whose ends are attached to a frame. The beam length is $0.0125\,m$ and its square section is $0.001 \times 0.001\,m^2$. The exterior dimensions of the cube are $0.005 \times 0.005 \times 0.005\,m^3$. The hole is a cylinder that is centered in the cube for which the dimensions are $0.005 \times 0.00175^2\pi\,m^3$. The material of the inclusion and of the frame is in ABS. This inclusion is manufactured using a 3D printing system (the ABS (Acrylonitrile Butadiene Styrene) is commonly used as a material for 3D printing). A steel screw is inserted in the hole (see Figure 1). The mass m of the inclusion is approximated by the mass of the screw that
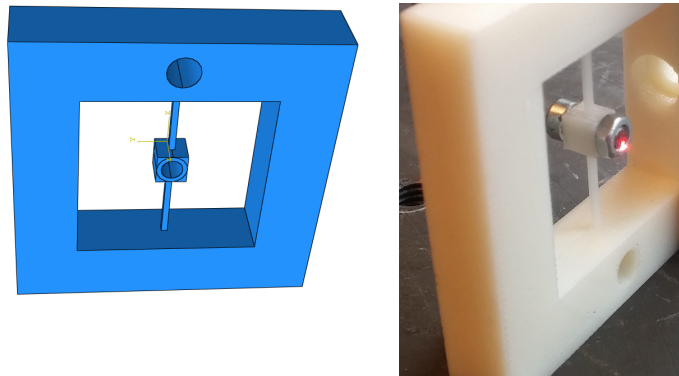

Figure 1. Design of the inclusion inserted in the frame (left figure) and its manufacturing with a 3D printing system (right figure).

is $0.0012\,kg$. The mass density of the ABS is $1,780\,kg/m^3$. Some experimental traction tests have been carried out for identifying the mechanical properties of the ABS material which is

assumed to be homogeneous, linear elastic and isotropic. The experiments yield for the Young modulus, $2.2 \times 10^9\,Pa$ and for the Poisson coefficient 0.35. This inclusion has been designed in order that the first eigenfrequency of the frame be around $1,200\,Hz$ and the first eigenfrequency of the inclusion (point mass and beam) be around $167\,Hz$. We are interested in analyzing the stationary random response of the inclusion in the frequency band of analysis $B_a = [-f_{\max}, f_{\max}]$ with $f_{\max} = 1,024\,Hz$, induced by the stationary random excitation generated by an imposed acceleration of the two ends supports of the beam. The same acceleration is imposed to the two supports. This acceleration is equal to the acceleration that is imposed to the frame (that can be considered as rigid in the frequency band of analysis), on which a stationary random external force is applied (see Section 5). The frequency band that is observed is the band $B_o = [90, 190]\,Hz \subset B_a$, which contains the resonance frequency for the low and the high amplitudes of the excitation.

3. Computational model with stochastic excitation

As explained in Section 1, a nonlinear oscillator with one DOF is constructed for modeling the nonlinear dynamical behavior of the inclusion defined in Section 2. The nonlinearity of the inclusion is due to nonlinear geometrical effects induced by finite displacements, the ABS material staying with a linear behavior. For the experimental configuration that is studied, the principal direction of the excitation and of the measured response of the inclusion is according to the normal displacement to the plane defined by the frame (bending of the beam in the plane perpendicular to the plane of the frame). Consequently, the proposed approach consists in modeling this normal displacement of the inclusion by a one-DOF nonlinear oscillator. As the nonlinearity is due to geometrical effects due to finite displacement, it could be expected a hardening effect that would induce an increase of the resonance frequency. However, the experimental measurements performed for this inclusion (see Section 5) have shown a softening behavior for which the resonance frequency significantly decreases. Such behavior can only be explained by the participation of other displacement DOFs (torsion around the axis of the beam and in plane bending displacement that is in the plane of the frame), which are excited by a nonlinear coupling. Consequently, for this type of behavior, it would be better to develop a multi-DOFs nonlinear oscillator (which is in progress as the step two of the work). Nevertheless, it is interesting to develop a one-DOF nonlinear oscillator for which the nonlinear elastic force is directly identified by using the experimental results. Such an identified model, which will approximatively reproduce the measurements, will allow to analyze the expected phenomena of the energy pumping over a broader frequency band around the resonance frequency.

The one-DOF nonlinear model is composed of a mass-spring-damper system with a nonlinear spring, excited by its support (see the scheme displayed in Figure 2). The mass of the beam is neglected. Let $X_{\mathrm{imp}}^{\mathrm{exp}}(t)$ be the displacement imposed at the support in the absolute frame and let $X_s(t)$ be the relative displacement of the point mass with respect to the support. Let $\{\ddot{X}_{\mathrm{imp}}^{\mathrm{exp}}(t), t \in \mathbb{R}\}$ be the acceleration imposed to the support, which is a Gaussian stationary second-order centered stochastic process, defined on the probability space $(\Theta, \mathcal{T}, \mathcal{P})$, for which the power spectral density function is denoted by $S_{\ddot{X}_{\mathrm{imp}}^{\mathrm{exp}}}(\omega)$. We aim to find the stationary second-order stochastic solution $\{X_s(t), t \in \mathbb{R}\}$ (which is not Gaussian) of the following stochastic nonlinear equation $m(\ddot{X}_s(t) + \ddot{X}_{\mathrm{imp}}^{\mathrm{exp}}(t)) + c\dot{X}_s(t) + \Phi'(X_s(t)) = 0$ for t in $\mathbb{R}$, which is rewritten as

$$m\ddot{X}_s(t) + c\dot{X}_s(t) + \Phi'(X_s(t)) = F_s^{\mathrm{exp}}(t), \ t \in \mathbb{R}, \tag{1}$$

in which $F_s^{\mathrm{exp}}(t) = -m\,\ddot{X}_{\mathrm{imp}}^{\mathrm{exp}}(t)$, where m is the mass of the inclusion introduced before, c is the damping coefficient, $\Phi'(x)$ is the derivative with respect to x of the elastic potential which will be identified in Section 5 for two different amplitudes of the excitation.
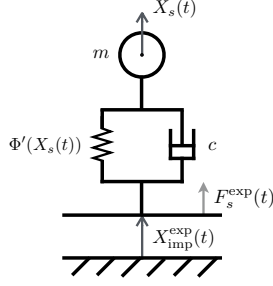
Figure 2. 1D simplified model.

The mean input power $\Pi_{\text{in}} = E\{F_s^{\text{exp}}(t)\,\dot{X}_s(t)\}$ (in which E is the mathematical expectation) and the mean power dissipated $\Pi_{\text{diss}} = c\,E\{\dot{X}_s(t)^2\}$, which are independent of t and which are equal (due to the stationarity), can be written as $\Pi_{\text{in}} = \int_{\mathbb{R}} \pi_{\text{in}}(\omega)\,d\omega$ and $\Pi_{\text{diss}} = \int_{\mathbb{R}} \pi_{\text{diss}}(\omega)\,d\omega$, in which the density $\pi_{\text{in}}(\omega)$ and $\pi_{\text{diss}}(\omega)$ are such that

$$\pi_{\text{in}}(\omega) = S_{F_s^{\text{exp}}\dot{X}_s}(\omega) \quad , \quad \pi_{\text{diss}}(\omega) = c\,S_{\dot{X}_s}(\omega). \tag{2}$$

In Eq. (2), $S_{F_s^{\text{exp}}\dot{X}_s}$ is the cross-spectral density function of the stationary stochastic processes F_s^{exp} and $\dot{X}_s$, and $S_{\dot{X}_s}$ is the power spectral density function of the stationary stochastic process $\dot{X}_s$. The energy pumping expressed as a function of the frequency is therefore characterized by $\pi_{\text{in}}(\omega) = \pi_{\text{diss}}(\omega)$. In order to qualify the efficiency of this energy pumping as a function of the intensity of the nonlinearity, we introduce the normalized quantity,

$$\pi_{\text{in,norm}}(\omega) = \frac{\pi_{\text{diss}}(\omega)}{S_{F_s^{\text{exp}}}(\omega)} . \tag{3}$$

Finally, the elastic potential $\Phi(x)$ will be experimentally identified by using the frequency dependent function $\text{FRF}^2(\omega)$ defined on B_0 by,

$$\text{FRF}^2(\omega) = \frac{|S_{\dot{X}_s F_s^{\text{exp}}}(\omega)|^2}{|S_{F_s^{\text{exp}}}(\omega)|^2} \tag{4}$$

It should be noted that if $\Phi'(x)$ was a linear function of x (linear oscillator), then FRF^2 would represent the square of the modulus of the frequency response function of the associated linear filter for which F_s^{exp} is the input and $\dot{X}_s$ is the output.

4. Stochastic solver and signal processing

Stochastic solver. For constructing the stationary stochastic solution of the nonlinear differential equation Eq. (1), the Monte Carlo method [29] is used. Let $\{F_s^{\text{exp}}(t;\theta_\ell), t \in \mathbb{R}\}$ be a realization of the stochastic process F_s^{exp} for $\theta_\ell \in \Theta$. Considering L independent realizations, for each realization θ_ℓ, we then have to solve the deterministic nonlinear differential equation with initial conditions,

$$\begin{cases} m\ddot{X}(t;\theta_\ell) + c\dot{X}(t;\theta_\ell) + \Phi'(X(t;\theta_\ell)) = F_s^{\text{exp}}(t;\theta_\ell), \ t \in [0, t_0 + T], \\ X(0,\theta_\ell) = 0, \ \dot{X}(0,\theta_\ell) = 0. \end{cases} \tag{5}$$

The part $\{X(t;\theta_\ell), t \in [0, t_0]\}$ of the non-stationary random response corresponds to the transient signal induces by the initial conditions, that decreases exponentially due to the damping.

This part of the response is removed in the signal processing of the second-order quantities of the stationary solution. Time t_0 is chosen in order that the transient response be negligible for $t \geq t_0$. The part of the trajectory corresponding to the stationary response is $X_s(t; \theta_\ell) = X(t - t_0; \theta_\ell)$ for t in $[t_0, t_0 + T]$. The time duration T that is related to the frequency resolution is defined after. The deterministic problem defined by Eq. (5) will be solved with a Störmer-Verlet scheme presented after.

Time and frequency sampling. For constructing the second-order quantities of the stationary response X_s, the signal processing requires a time sampling with a constant time step Δ_t that is performed using the Shannon theorem for the stationary stochastic processes [30, 31]. The sampling frequency is thus written as $f_e = 2 f_{\max}$ and the time step is $\Delta_t = 1/f_e$. The corresponding time sampling is $t_\alpha = \alpha \Delta_t$ with $\alpha = 0, 1, ..., N - 1$ in which the integer N is chosen in order that the frequency resolution $\Delta_f = 1/T = 0.125 \, Hz$ where $T = N\Delta_t$ yielding $N = 16,384$ for $T = 8 \, s$. The corresponding sampling points in the frequency domain are $f_\beta = -f_{\max} + (\beta + 1/2)\Delta_f$ for $\beta = 0, 1, ..., N - 1$.

Generation of independent realizations of stochastic process F_s^{exp}. The usual second-order spectral representation of the stationary stochastic processes is used [32, 33]. The power spectral density function $S_{F_s^{\mathrm{exp}}}(\omega)$ of the Gaussian stationary second-order centered stochastic process F_s^{exp} is such that $S_{F_s^{\mathrm{exp}}}(\omega) = m^2 \, S_{\ddot{X}_{\mathrm{imp}}^{\mathrm{exp}}}(\omega)$, in which $S_{\ddot{X}_{\mathrm{imp}}^{\mathrm{exp}}}(\omega) = \omega^4 \, S_{X_{\mathrm{imp}}^{\mathrm{exp}}}(\omega)$. The autocorrelation function $\tau \mapsto R_{\ddot{X}_{\mathrm{imp}}^{\mathrm{exp}}}(\tau)$ of stochastic process $\ddot{X}_{\mathrm{imp}}^{\mathrm{exp}}$ is such as $R_{\ddot{X}_{\mathrm{imp}}^{\mathrm{exp}}}(\tau) = E\{\ddot{X}_{\mathrm{imp}}^{\mathrm{exp}}(t + \tau)\ddot{X}_{\mathrm{imp}}^{\mathrm{exp}}(t)\}$ and is such that $R_{\ddot{X}_{\mathrm{imp}}^{\mathrm{exp}}}(\tau) = \int_R e^{i\omega\tau} S_{\ddot{X}_{\mathrm{imp}}^{\mathrm{exp}}}(\omega) \, d\omega$. The generator of realizations of the Gaussian stationary second-order stochastic process $\ddot{X}_{\mathrm{imp}}^{\mathrm{exp}}$ is based on the usual spectral representation [34, 35]. Let $\Psi_0, \ldots, \Psi_{N-1}$ be N mutually independent uniform random variables on $[0, 1]$, and let $\phi_0, \ldots, \phi_{N-1}$ be N mutually independent uniform random variables on $[0, 2\pi]$, which are independent of $\Psi_0, \ldots, \Psi_{N-1}$. The spectral representation used is,

$$\ddot{X}_{\mathrm{imp}}^{\mathrm{exp}}(t) \simeq \sqrt{2\Delta_\omega} \, \mathrm{Re}\Big\{ \sum_{\beta=0}^{N-1} \sqrt{S_{\ddot{X}_{\mathrm{imp}}^{\mathrm{exp}}}(\omega_\beta)} \, Z_\beta \, e^{-i\omega_\beta t} \, e^{-i\phi_\beta} \Big\}, \; t \in [0, t_0 + T] \;, \qquad (6)$$

in which $\Delta_\omega = 2\pi \Delta_f$, where $Z_\beta = \sqrt{-\log(\Psi_\beta)}$ and $\omega_\beta = 2\pi f_\beta$. From Eq. (6), it can be deduced that the realization $\{\ddot{X}_{\mathrm{imp}}^{\mathrm{exp}}(t; \theta_\ell), t \in [t_0; t_0 + T]\}$ is written as

$$\ddot{X}_{\mathrm{imp}}^{\mathrm{exp}}(t; \theta_\ell) \simeq \sqrt{2\Delta_\omega} \, \mathrm{Re}\Big\{ \sum_{\beta=0}^{N-1} g_{\beta,\ell} \, e^{-i\omega_\beta t} \Big\}, \; t \in [0, t_0 + T] \,, \qquad (7)$$

in which $g_{\beta,\ell} = \sqrt{S_{\ddot{X}_{\mathrm{imp}}^{\mathrm{exp}}}(\omega_\beta)} \, Z_\beta(\theta_\ell) \, e^{-i\phi_\beta(\theta_\ell)}$. Introducing the FFT $\{\widehat{g}_{0,\ell}, \ldots, \widehat{g}_{N-1,\ell}\}$ of $\{g_{0,\ell}, \ldots, g_{N-1,\ell}\}$, which is written as $\widehat{g}_{\alpha,\ell} = \sum_{\beta=0}^{N-1} g_{\beta,\ell} \exp\{-2i\pi\,\alpha\beta/N\}$ for $\alpha = 0, 1, ..., N-1$, we obtain

$$\ddot{X}_{\mathrm{imp}}^{\mathrm{exp}}(t_\alpha; \theta_\ell) = \sqrt{2\Delta_\omega} \, \mathrm{Re}\Big\{ \exp\{-i\pi\alpha\big(\frac{1-N}{N}\big)\} \widehat{g}_{\alpha,\ell} \Big\} \,, \alpha = 0, 1, \ldots, N-1 \,. \qquad (8)$$

Störmer-Verlet integration scheme. The Störmer-Verlet integration scheme is well suited for the resolution of dynamical Hamiltonian systems [36, 37] as proposed, for instance, for the dissipative case, in [38]. Such a scheme preserves the mechanical energy during the numerical integration.

We thus rewrite Eq. (5) in the following dissipative Hamiltonian form as

$$
\begin{cases}
\dot{X}(t;\theta_\ell) = \dfrac{1}{m}\,Y(t;\theta_\ell) \quad , \quad t \in [t_0, t_0 + T]\,, \\[2ex]
\dot{Y}(t;\theta_\ell) = -\Phi'(X(t;\theta_\ell)) - \dfrac{c}{m}\,Y(t;\theta_\ell) + F_s^{\mathrm{exp}}(t;\theta_\ell) \quad , \quad t \in [t_0, t_0 + T]\,, \\[2ex]
X(0;\theta_\ell) = 0 \,,\ \ Y(0;\theta_\ell) = 0\,.
\end{cases}
\tag{9}
$$

We use the notation $u_\ell^\alpha = U(t_\alpha;\theta_\ell)$. The Störmer-Verlet integration scheme for Eq. (9) is then written, for $\alpha = 0, 1, ..., N - 1$, as

$$
\begin{cases}
x_\ell^{\alpha+1/2} = x_\ell^\alpha + \dfrac{\Delta_t}{2m}\,y_\ell^\alpha\,, \\[2ex]
y_\ell^{\alpha+1} = y_\ell^\alpha + \Delta_t\left(-\Phi'(x_\ell^{\alpha+1/2}) - \dfrac{c}{2m}\,y_\ell^\alpha - \dfrac{c}{2m}\,y_\ell^{\alpha+1} + F_s^{\mathrm{exp}}(t_{\alpha+1};\theta_\ell)\right)\,, \\[2ex]
x_\ell^{\alpha+1} = x_\ell^{\alpha+1/2} + \dfrac{\Delta_t}{2m}\,y_\ell^{\alpha+1}\,,
\end{cases}
\tag{10}
$$

in which $F_s^{\mathrm{exp}}(t_{\alpha+1};\theta_\ell) = -m\ddot{X}_{\mathrm{imp}}^{\mathrm{exp}}(t_{\alpha+1};\theta_\ell)$.

Signal processing. For estimating, the power spectral density functions and the cross-spectral density functions defined in Eqs. (2) and (4), the periodogram method [30, 31] is used.

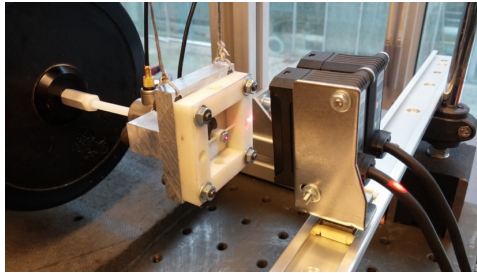## 5. Experimental measurements and identification of the model with stochastic excitation

Figure 3. The experimental configuration.

Experimental configuration and measurements. The experimental configuration can be viewed in Figure 3. The displacement $X_{\mathrm{imp}}^{\mathrm{exp}}$ at a point of the rigid frame that is suspended and the displacement X^{exp} of the point mass (inclusion) are measured with two laser sensors. The excitation applied to the rigid frame is done by a shaker. The experimental responses have been measured for two amplitudes of the experimental accelerations $\ddot{X}_{\mathrm{imp}}^{\mathrm{exp}}$: the first one corresponds to a low amplitude for which the response of the oscillator is approximately linear and the second one corresponds to a high amplitude for which the response is nonlinear. These two cases will be identified by symbols L and NL, respectively. Consequently, the corresponding force $F_s^{\mathrm{exp}} = -m\,\ddot{X}_{\mathrm{imp}}^{\mathrm{exp}}$ applied to the oscillator is denoted, for the two amplitudes, by $F_s^{\mathrm{exp,L}}$ and $F_s^{\mathrm{exp,NL}}$. The power spectral density functions $S_{F_s^{\mathrm{exp,L}}}$ and $S_{F_s^{\mathrm{exp,NL}}}$ are displayed in Figure 4 for the frequency band B_o. Some fluctuations can be seen in these power spectral density functions, which

imply some fluctuations in the power spectral density functions of the inclusion displacement (these fluctuations will be reduced for the future works by adapting the experimental configuration and the signal processing). As these experimental power spectral density functions are used as input for computing the stochastic responses of the nonlinear oscillator, these fluctuations induce some fluctuations in the power spectral density functions of the responses.
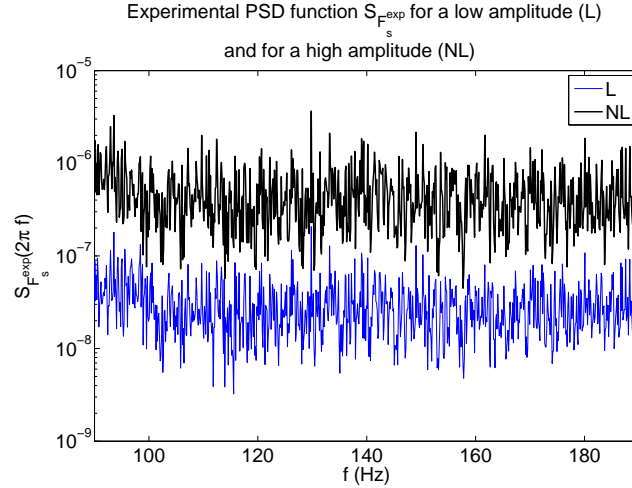

Figure 4. Experimental PSD function $S_{F_x}^{exp}$ for a low amplitude (L) and for a high amplitude (NL) of the excitation.

Experimental identification of the nonlinear elastic force. As explained in Section 3, for each one of the two amplitudes, the experimental identification of the nonlinear elastic force is performed by minimizing over the frequency band B_o, the distance between FRF^2 (defined by Eq. (6)) computed with the model and the same quantity constructed with the experimental measurements.

(i)- *Low amplitude.* A one-parameter algebraic representation of $\Phi'(x)$ is chosen as $\Phi'_{L}(x) = k_1 x$. The experimental identification gives $k_1 = 1,305\,N/m$ (see Figure 5).

(ii)- *High amplitude.* A three-parameters algebraic representation of $\Phi'(x)$ is defined by $\Phi'_{NL}(x) = k_1 x (\alpha_1 + \alpha_2 x^2)^{-1/4}$ in which k_1 is fixed to the value identified for the low-amplitude case and where the experimental identification of the two positive parameters α_1 and α_2 yields $\alpha_1 = 3$ and $\alpha_2 = 10^8\,m^{-2}$ (see Figure 5).

For each one of the two amplitudes, Figure 6 displays the comparison of the FRF^2 function for the identified model with that obtained with the experiments. It can be seen a reasonable agreement between the experiments and the computation, knowing that an approximation has been introduced for constructing the model (see the explanations given in Section 3) and in taking to account the existence of fluctuations in the experimental power spectral density function of the input.

6. Energy pumping in frequency band B_o and comparison with the experiments

Figure 7 (predictions with the identified model) and Figure 8 (experiments) display the normalized input power density defined by Eq. (3) for the low amplitude and for the high amplitude. It can be seen a reasonable agreement between the prediction with the model and the experiments. Nevertheless, the results presented in these two figures confirm a strong effect
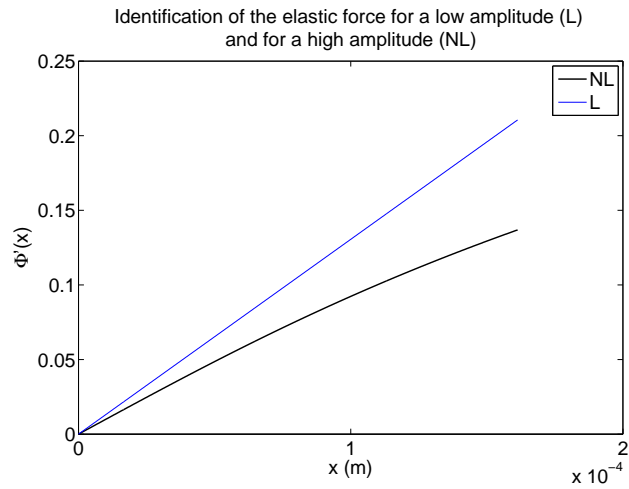
Figure 5. Identification of the elastic force for a low amplitude (L) and for a high amplitude (NL) of the excitation.
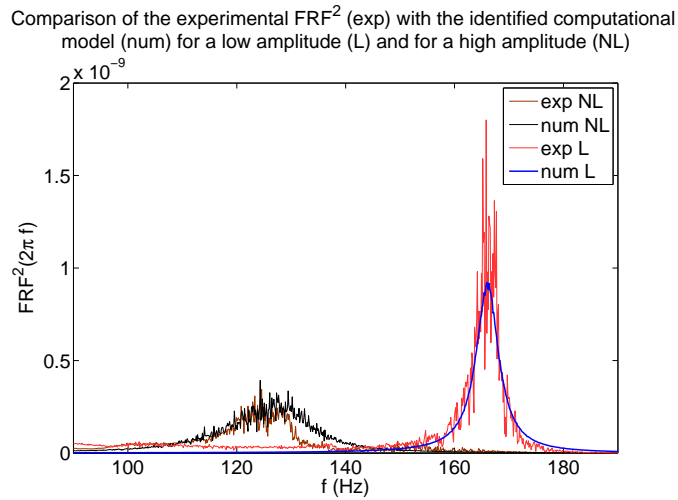

Figure 6. Comparison of the experimental FRF^2 (exp) with the identified computational model (num) for a low amplitude (L) and for a high amplitude (NL).

of the nonlinearity that allows the pumping energy phenomenon to be efficient over a broader frequency band around the resonance frequency than for the linear case, which was the objective of the work.

7. Conclusions

In this paper, we have presented the results related to the first step of a work devoted to the design and the analysis of a nonlinear microstructured material to reduce noise and vibrations at low frequencies. We have developed the design of an inclusion at macroscale, which has been manufactured with a 3D printing system. The dimension of this inclusion can easily be reduced
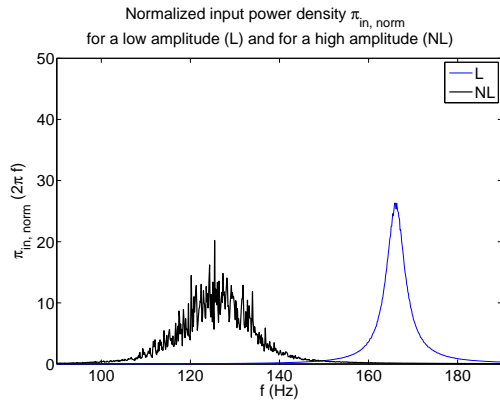
Figure 7. Normalized input power density $\pi_{\mathrm{in,norm}}$ for the low amplitude (L) and for the high amplitude (NL).
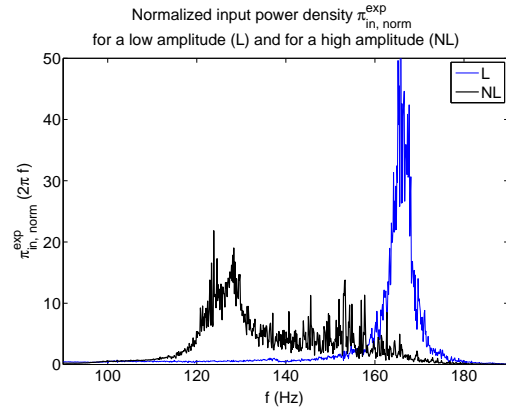

Figure 8. Normalized input power density $\pi_{\mathrm{in,norm}}^{exp}$ for the low amplitude (L) and for the high amplitude (NL).

with the same technology. A first version of a nonlinear dynamical model has been developed and its parameters have been identified with the experiments. Both the predictions given by the model and the experiments confirm that the pumping energy phenomenon is more efficient over a broader frequency band around the resonance frequency than for the linear case. The work in progress is the development of a more sophisticated model of the inclusion, which takes into account the nonlinear couplings between several degrees of freedom.

Acknowledgments

References

[1] Frahm H 1911 *United states patent office* 1–9
[2] Roberson R E 1952 *Portions of a dissertation submitted to the Department of Applied Mechanics, Washington University, in partial fulfillment of the requirements for the degree of Doctor of Philosophy.* 205–220
[3] Smith D and Kroll N 2000 *Physical Review Letters* **85** 2933–2936
[4] Chen H and Chan C 2007 *Applied Physics Letters* **91** 183518–1, 183518–3
[5] Ding Y, Liu Z, Qiu C and Shi J 2007 *Physical Review Letters* **99** 093904–1, 093904–4
[6] Sheng P, Mei J, Liu Z and Wen W 2007 *Physica B* **394** 256–261
[7] Yang Z, Mei J, Yang M, Chan N and Sheng P 2008 *Physical Review Letters* **101(20)** 204301–1, 204301–4
[8] Lee S, Park C, Seo Y, Wang Z and Kim C 2009 *Physics Letters A* **373** 4464–4469
[9] Zhou X and Hu G 2009 *Physical Review B* **79** 195109–1, 195109–9
[10] Liu X, Hu G, Huang G and Sun C 2011 *Applied Physics Letters* **98** 251907
[11] Li, S and Gao, XL (eds) 2013 *Handbook of Micromechanics and Nanomechanics* (Pan Stanford Publishing)
[12] Hussein M and Frazize M 2013 *Journal of Sound and Vibration* **332** 4767–4774
[13] Del Vescovo D and Giorgio I 2014 *International Journal of Engineering Science* **80** 153–172
[14] Wang X 2014 *International Journal of Solids and Structures* **51** 1534–1541
[15] Zhu R, Liu X, Hu G, Sun C and Huang G 2014 *Journal of Sound and Vibration* **333** 2759–2773
[16] Wang X, Zhao H, Luo X and Huang Z 2016 *Applied Physics Letters* **108(4)** 041905
[17] Soize C 1995 *Computers and Structures* **58** 901–915
[18] Gendelman O, Manevitch L, Vakakis A and MCloskey R 2001 *Journal of Applied Mechanics* **68** 34–41
[19] Vakakis A and Gendelman O 2001 *Journal of Applied Mechanics* **68** 42–48
[20] Vakakis A 2003 *Journal of Vibration and Control* **9** 79–93
[21] Milton G, Briane M and Willis J 2006 *New Journal of Physics* **8** 1–20
[22] Carrella A, Brennan M and Waters T 2007 *Journal of Sound and Vibration* **301** 678–689

[23] Alexander N and Schilder F 2009 *Journal of Sound and Vibration* **319** 445–462
[24] Yang Z, Dai H, Chan N, Ma G and Sheng P 2010 *Applied Physics Letters* **96** 041906–1, 041906–3
[25] Auriault J L and Boutin C 2012 *International Journal of Solids and Structures* **49** 3269–3281
[26] Xiao Y, Wen J and Wen X 2012 *Journal of Sound and Vibration* **331** 5408–5423
[27] Varanasi S, Bolton J, Siegmund T and Cipra R 2013 *Applied Acoustics* **74** 485–495
[28] Viet L and Nghi N 2014 *Engineering Structures* **81** 175–180
[29] Rubinstein R and Kroese D 2008 *Simulation and the Monte Carlo Method* (Second Edition, John Wiley & Sons)
[30] Papoulis A 1965 *Probability, Random Variables and Stochastic Processes* (McGraw-Hill, New York)
[31] Soize C 1997 Fundamentals of Random Signal Analysis, Application to Modal Identification in Structural Dynamics, Course given at PUC-Rio University, Rio de Janeiro, Brazil, August 19-23, 1996. Final Edition, Paris, France
[32] Guikhman L and Skorokhod A 1979 *The Theory of Stochastic Processes* (Springer Verlag)
[33] Priestley M 1981 *Spectral Analysis and Time Series* (Academic Press, New York)
[34] Shinozuka M 1971 *Journal of the Acoustical Society America* **49** 357–367
[35] Poirion F and Soize C 1995 *Probabilistic Methods in Applied Physics* ed Krée P and Wedig W (Springer-Verlag, Berlin) pp 17–53
[36] Verlet L 1967 *Physical Review* **159** 98–103
[37] Hairer E, Lubich C and Wanner G 2003 *Acta Numerica* **12** 399–450
[38] Soize C and Poloskov I E 2012 *Computers and Mathematics with Applications* **64** 3594–3612